

Conditions for the Thermal Instability in the Galactic Centre Mini-spiral region

A. Różańska^{1*}, B. Czerny¹, D. Kunneriath², T. P. Adhikari¹, V. Karas², M. Mościbrodzka³

¹ *N. Copernicus Astronomical Center, Bartycka 18, 00-716 Warsaw, Poland*

² *Astronomical Institute, Academy of Sciences, Boční II 1401, CZ-14131 Prague, Czech Republic*

³ *Department of Astrophysics/IMAPP, Radboud University Nijmegen, P.O. Box 9010, 6500 GL Nijmegen, The Netherlands*

Accepted

ABSTRACT

We explore the conditions for the thermal instability to operate in the mini-spiral region of the Galactic centre (Sgr A*), where both the hot and cold media are known to coexist. The photoionisation Cloudy calculations are performed for different physical states of plasma. We neglect the dynamics of the material and concentrate on the study of the parameter ranges where the thermal instability may operate, taking into account the past history of Sgr A* bolometric luminosity. We show that the thermal instability does not operate at the present very low level of the Sgr A* activity. However, Sgr A* was much more luminous in the past. For the highest luminosity states the two-phase medium can be created up to 1.4 pc from the centre. The presence of dust grains tends to suppress the instability, but the dust is destroyed in the presence of strong radiation field and hot plasma. The clumpiness is thus induced in the high activity period, and the cooling/heating timescales are long enough to preserve later the past multi-phase structure. The instability enhances the clumpiness of the mini-spiral medium and creates a possibility of episodes of enhanced accretion of cold clumps towards Sgr A*. The mechanism determines the range of masses and sizes of clouds; under the conditions of Sgr A*, the likely values come out $1\text{--}10^2 M_{\odot}$ for the cloud typical mass.

Key words: instabilities – methods: numerical – ISM: structure – ISM: clouds – Galaxy: centre

1 INTRODUCTION

The thermal instability can develop when an interstellar medium is irradiated by sufficiently intense external source. In a certain range of parameters multiple phases can arise and thermally different states can stay in thermal equilibrium (Field 1965). Near a supermassive black hole a two-phase medium forms spontaneously at certain range of the central luminosities and distances from the centre (Krolik et al. 1981).

The interstellar medium has a complex multiphase structure which is not yet fully understood (for review, see Cox 2005). This structure is important from the point of view of feeding the Milky Way's central supermassive black hole as well as the possibility of an accompanying outflow. A similar mechanism is expected to operate in the other low luminosity galactic nuclei.

Some aspects of this multiphase structure were already studied by Field (1965) who considered the thermal equilibrium of the radiatively heated and cooled plasma. He showed that for a certain range of the parameters the plasma is thermally unstable, and the colder, denser matter may coexist with the rarefied hot

medium in pressure equilibrium due to different cooling/heating mechanisms dominating at high and low gas densities. This theory was further developed in a number of papers, where the effect of steady evaporation or condensation of the cold phase was taken into account (Cowie & McKee 1977; McKee & Cowie 1977; Begelman et al. 1983; Begelman & McKee 1990). The thermal instability and eventual cloud evaporation predominantly depend on the heating and cooling processes taken into account in the energy equilibrium equation. In the case of illuminated accretion disks viscous heating should be considered (Różańska & Czerny 1996; Różańska 1999).

The next major step was done in series of three papers (Barai et al. 2011, 2012; Mościbrodzka & Proga 2013), where the authors combined the simple theory of spherical (Bondi) accretion with the theory of radiative instability due to preheating of the accretion flow by the X-ray flux generated by accretion close to the black hole. In all three papers, the authors performed careful numerical simulations of the dynamics of the accretion flow with the proper treatment of heating/cooling mechanisms. These results showed that a two-phase medium formed spontaneously at some ranges of the central luminosity/distance from the black hole (Barai et al. 2011), the colder clumps formed filaments which ac-

* E-mail: agata@camk.edu.pl

creted faster than the surrounding hot plasma (Barai et al. 2012). These filaments may break into smaller cloudlets, which may be revealed only if numerical method allows for the required resolution (Mościbrodzka & Proga 2013).

The Milky Way interstellar medium is the best studied case of complex cosmic environment, and the multi-phase region in the close vicinity of the central massive black hole is clearly detected (Zhao et al. 2009). The accretion onto Sgr A* is very complex, not only due to the hot Bondi-type flow but also likely due to occasional accretion events of colder clumps. The argument for the second aspect comes both from the currently observed approach of the G2 cloud and also from the observed X-ray echo from the large molecular clouds surrounding Sgr A* which allows to constrain much higher activity of Galactic centre (GC) in the past (Sunyaev et al. 1993; Koyama et al. 1996; Ponti et al. 2010; Capelli et al. 2012). The time profile of this activity level with rather large luminosity, of order of 10^{40} erg s⁻¹ for a few hundred years followed by a rapid fast decay is not easy to model, and the suggested explanation was through an accretion of a chain of similar clouds (Czerny et al. 2013b). Thus the question appears whether the mechanism considered by Barai et al. (2011, 2012) and Mościbrodzka & Proga (2013) can indeed apply to the central parts of Sgr A* and drive this behaviour.

Czerny et al. (2013a) emphasize that the amount of material contained in the mini-spiral is sufficient to sustain the past luminosity of Sgr A* at the required level. The accretion episodes of relatively dense gas from the mini-spiral passing through a transient accretion ring at about 10^4 gravitational radii of the supermassive black hole provide a viable scenario for the bright phase of the Galactic center. What remains to clarify is an important aspect of the mechanism of the angular momentum loss that must operate in order to bring this material further down to the horizon.

The observations of the circumnuclear region of Sgr A* show a reservoir of cold clumps in the mini-spiral. This material has a rather high angular momentum so the whole picture is more complex than the quasi-spherical dynamical setup of the previous works. Therefore, in the present paper we entirely neglect the dynamics of the material and concentrate on the simple study of the parameter ranges where the thermal instability may operate, taking into account the varying X-ray flux of Sgr A* in the past few hundred years. Our approach is complementary to numerical simulations (Alig et al. 2013), where the authors argue that the mini-spiral itself formed in a collision of a molecular cloud with the circumnuclear disk. We show how those clouds can form due to thermal instabilities in the strong radiation field.

We use Cloudy¹ photoionisation code (Ferland et al. 2013) to: (i) set up a simplified model of the ISM in the GC to investigate the conditions required to obtain accretion driven by thermal instabilities, (ii) calculate instability curves for different luminosity states of Sgr A* to determine if its past high luminosity state inferred from X-ray reflection clouds is sufficient to create a two-phase medium in the mini-spiral region, (iii) study the influence of dust grains in the mini-spiral region on the creation of thermal instabilities.

We show that for the highest luminosity states, the two-phase medium can be created up to 1.4 pc away from the GC. Timescales of most clouds are of the order of 10^{2-6} years, depending on the cloud density. The extent of the two-phase medium depends on the value of gas pressure of the hot phase plasma. Adopting the gas pressure, of a typical Bondi flow, we calculated instability strips

for several highest-luminosity states of Sgr A*. Finally, we demonstrate that the dust content does not allow the emergence of thermal instability, but on the other side, dust should quickly evaporate in such hot Bondi flow (Draine & Salpeter 1979).

The structure of the paper is as follows: in Sec. 2 we summarize the morphology of the mini-spiral known from current observations, in Sec. 3 we describe the method of photoionisation calculations. All results are presented in Sec. 4, 5, and discussed in Sec. 6. Final conclusions are given in Sec. 7.

2 THE MATERIAL CONTENT OF THE MINI-SPIRAL

The interstellar medium in the central 10 pc of the GC is a complex mixture of ionized, neutral and molecular gas, and dust that is heated up by its interaction with the central supermassive black hole, Sgr A*, and also directly by the stars in the Nuclear Stellar Cluster (NSC) in the region. The circumnuclear disc is a ring of $\approx 10^5 M_\odot$ of neutral atomic and molecular material (see Vollmer & Duschl 2002; Christopher et al. 2005, and references therein) extending from about 1.5-10 pc, which encompasses Sgr A West, the thermal HII emission region, the brightest part of which is the so-called mini-spiral. The mini-spiral consists of three streams of ionized gas (the Northern Arm, Eastern Arm and the Western Arc), with most of the gas predominantly in a Keplerian orbit with observed radial velocity components spanning from +200 to -415 km/s, with a few significant deviations. The Northern and Eastern arms appear to collide about 0.1-0.2 pc behind Sgr A* (Zhao et al. 2010). The partially ionized gas in the mini-spiral arms have number densities ranging $3-21 \times 10^4$ cm⁻³, with temperatures in the interval 5000-13 000 K (Zhao et al. 2009). The mini-spiral also contains dust with temperatures in the range of 200-300 K (Cotera et al. 1999). The fraction of material in the form of dust is low ($\sim 0.50 M_\odot$) for the central 1.5×1.5 parsec region (Gezari et al. 1985) when compared to the $\sim 160 M_\odot$ ionized gas in the central 3×3 pc region (Liszt 2003).

From the *Chandra* data (Baganoff et al. 2003), we have an estimate of local density and temperature of the hot, fully ionized plasma: direct map analysis implies $n_e = 130$ cm⁻³, $T_e = 2$ keV at 1.5'' (i.e. 0.06 pc). Next, the modeling of emissivity profile in the very long *Chandra* data (Shcherbakov & Baganoff 2010) suggest $n_e = 90$ cm⁻³, $T_e = 2.5$ keV at this distance. Farther away, the density and temperature are lower: $n_e = 27$ cm⁻³, $T_e = 1.3$ keV at about 1 pc (Baganoff et al. 2003). On the other hand, from the spectral fitting of 134.77 ks *Chandra* observation, (Różańska et al. 2014, in preparation) estimated the electron temperature of the hot ionized gas to be $T_e = 3.5$ keV at 5'' (0.2 pc). On moving to the diffuse gas in the Sgr A East up to 60'' the average gas temperature is estimated to be $T_e = 3.1$ keV. The surface brightness modelling in the vicinity of the black hole (up to 3'', 0.12 pc) requires the Bondi accretion flow with outer temperature $T_e^{\text{out}} = 3.5$ keV and the electron density $n_e^{\text{out}} = 18.3$ cm⁻³ for the best fit with observed surface brightness. From this study, the density and temperature estimated at the distance of 1.5'' are $n_e = 29.2$ cm⁻³ and $T_e = 4.8$ keV respectively.

The two media (i.e., the hot ionized plasma and the partially ionized gas) appear to be in mutual contact and, to the first approximation, the pressure equilibrium is approximately established. This means that three orders of magnitude higher temperature of X-ray emitting plasma is compensated by its lower density. Below we model a two-phase medium using photoionisation calculations with

¹ <http://www.nublado.org/>

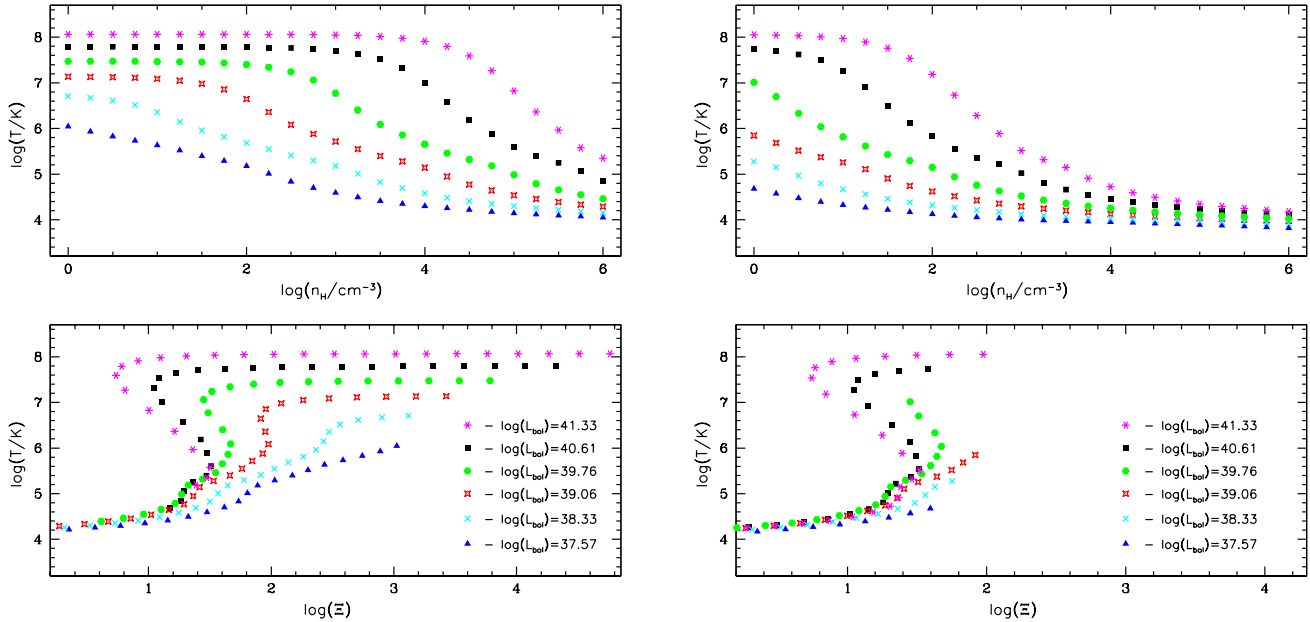


Figure 1. The comparison of thermal instability conditions at two different distances from the GC. Left panels show clouds located at $R_{in} = 0.008$, while the right panels exhibit clouds located at $R_{in} = 0.2$. The instability curves are presented in the lower panels, while the temperatures of those clouds versus their number densities are presented in upper panels for different luminosities.

a proper treatment of all cooling and heating mechanisms operating in both types of clouds.

3 THE METHOD

The thermal instability created due to radiative cooling and heating by the central black hole leads to the formation of a two-phase medium in the mini-spiral region, with the colder clumps of the mini-spiral structure breaking off and accreting into Sgr A*. This phenomenon can be modelled using photoionisation calculations where the radiation field interacts with matter due to bound-bound, bound-free and free-free processes. Therefore, we perform Cloudy calculations for initial conditions taken from observations done recently by working instruments. Cloudy solves the thermal structure, and emergent spectrum of the illuminated gas under the total ionisation equilibrium. Depending on the medium temperature and density, all ionisation and recombination processes are calculated for assumed abundances. Therefore, we can determine the total heat accumulated by the cloud due to irradiation, and follow up heating and cooling processes important under the given gas physical conditions.

The thermal instability is seen as a negative slope of the stability curve $\log(\Xi) - \log(T)$ (Krolik et al. 1981), where Ξ is the dynamical ionisation parameter, defined as the ratio of the radiation pressure to gas pressure:

$$\Xi = \frac{L_{\text{ion}}}{4\pi c R^2 k n_{\text{H}} T} = \frac{P_{\text{rad}}}{P_{\text{gas}}}, \quad (1)$$

where L_{ion} is the total ionizing luminosity, R the distance to the source, k is the Boltzmann constant, c the velocity of light, n_{H} hydrogen number density, and T is the temperature of the ionised medium.

The instability occurs if there is a range of values of the ionisation parameter Ξ for which the radiative balance equation has three different solutions of temperature. This can be illustrated by repeating calculations for clouds of different initial number densities n_{H} illuminated by the same radiation field.

We consider clouds of densities spanning from 1 up to $1.78 \times 10^6 \text{ cm}^{-3}$ (from 0 to 6.25 in log scale). Each cloud is located in the inner region of mini-spiral, which we estimate after Zhao et al. (2010) to be $R = 0.2 \text{ pc}$ ($\log(R/\text{cm}) = 17.79$) from GC. Assuming that the two-phase flow continues toward black hole, we consider also the case where clouds are closer at $R_{\text{in}} = 0.008 \text{ pc}$ ($\log(R_{\text{in}}/\text{cm}) = 16.35$) toward Sgr A*.

For each cloud, we assume open geometry, which means that the cloud is a thin shell with size ΔR , defined as $\Delta R/R = < 0.1$ in Cloudy options. In all calculations, we assume solar default abundances described by `hazy1.pdf2` documentation file. It was shown by Hess et al. (1997) that the unstable branch of stability curve is bigger for higher metal abundances. Especially, more iron is responsible for larger extent of the upper part of the stability curve, while more oxygen increases the thermal instability in the lower part of stability curve. Nevertheless, for the purpose of this paper we keep solar abundances.

For photoionisation calculations, the value of bolometric luminosity and the shape of illuminated radiation are crucial for the shape of stability curve. Since Sgr A* undergoes different luminosity states we have to consider all of them, which we describe in the subsection below.

² <http://www.nublado.org/>

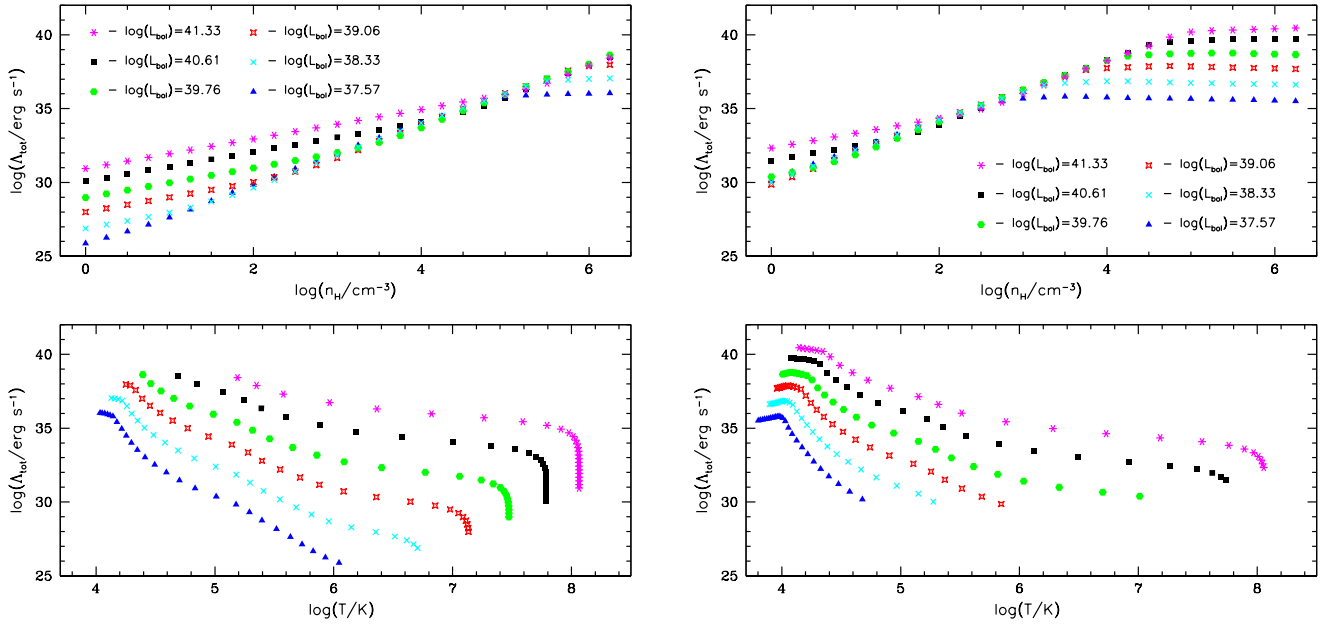


Figure 2. The comparison of total cooling rate of clouds at two different distances, as in Fig 1. Left panels show clouds located at $R_{in} = 0.008$, while right panels clouds located at $R_{in} = 0.2$. The total cooling rate versus temperature for different luminosities is presented in lower panels, while the dependence on cloud number density is presented in upper panels for both cases.

3.1 Luminosity states of Sgr A*

Sgr A* is highly underluminous, accreting at a rate of about 10^{-7} – 10^{-9} times the Eddington luminosity. The quiescent X-ray luminosity of Sgr A* is roughly 2×10^{33} erg s $^{-1}$, while in the flaring or active stage it is $\leq 10^{36}$ erg s $^{-1}$. The bolometric luminosity is considerably higher due to the strong near-IR and mm component. The bolometric luminosity in the past was a few orders of magnitude higher. Since we do not have the spectral shape of the Sgr A* radiation in the past, we use the theoretical models of GC by Mościbrodzka et al. (2012) computed for different accretion rates of radiatively inefficient accretion flow (RIAF). In those models the black hole mass was fixed at $M_{BH} = 4.5 \times 10^6 M_{\odot}$ (Ghez et al. 2008), and distance to the GC at $D = 8.4$ kpc (Gillessen et al. 2009). Mościbrodzka et al. (2012) computed spectra for accretion rates equal to: 1, 2, 4, 8, 16, 32, 64, and $128 \times 10^{-9} M_{\odot} \text{ yr}^{-1}$.

In photoionisation calculations we have considered all accretion rates, but for the figures presented in this paper we have chosen six states of bolometric luminosity: from the lowest one $\log(L_{bol}) = 37.57$, where the instability is not present – to the highest, $\log(L_{bol}) = 41.33$, where the instability is the strongest. Between those two extreme values we present also cases for: $\log(L_{bol}) = 38.33$, $\log(L_{bol}) = 39.06$, $\log(L_{bol}) = 39.76$, and $\log(L_{bol}) = 40.61$. The shape of each spectrum is taken from the typical hot accretion flow onto a supermassive black hole (for detailed prescription see Mościbrodzka et al. 2012).

The shape of the broad band spectrum for each luminosity state is given by points, using Cloudy “interpolate” command. Based on the output of Cloudy calculations we can determine ionization parameter, Ξ , of each cloud, the total heating rate per volume of the gas H_{tot} in erg s $^{-1}$ cm $^{-3}$, and the total cooling rate Λ_{tot} in erg s $^{-1}$, where the last value allows us to determine the cooling time according to the formula:

$$t_{cooling} = \frac{P_{gas}}{\Lambda_{tot}} = \frac{kn_{\text{H}}T}{\mu\Lambda_{tot}}, \quad (2)$$

where μ mean molecular weight = 0.5, as usual. Cloud temperature, T , is always self-consistently computed from photoionisation calculations.

Thermally unstable clouds would evaporate or condensate due to thermal instability and thermal conduction. If the heating/cooling curve shape implies the instability, the condensations will grow out of the initially uniform medium. Thermal conduction limits the smallest size of the clouds. It does not influence the size of thermal instability as it was shown by Begelman & McKee (1990); Różańska (1999). Taking into account classical thermal conductivity based on the assumption that the mean free path is short with respect to the temperature scale height, for plasma of cosmic abundance the conductivity is equal to $\kappa = 5.6 \times 10^{-7} T^{5/2}$ erg cm $^{-1}$ s $^{-1}$ K $^{-1}$ (Draine & Giuliani 1984). The size of such clouds can be estimated by Field length (Field 1965) which is a ratio of mean conductive flux to the total heating rate per volume:

$$\lambda_{\text{F}} = \left(\frac{5.6 \times 10^{-7} T^{7/2}}{H_{tot}} \right)^{1/2}. \quad (3)$$

The formation timescale of a cloud of this size is well approximated by Eq. 2 if the sound-crossing timescale across the cloud is much shorter than $t_{cooling}$ (Field 1965; Burkert & Lin 2000). The cloud size equal to Field length implies that the role of radiative cooling and conduction is comparable. In this case, if the external heating/cooling switches off, the cold cloud surrounded by the hot plasma will disappear due to the conduction in the same timescale.

On the other hand, we can simply estimate the total mass stored in the cloud:

$$M_{\text{C}} = m_{\text{H}} n_{\text{H}} V = m_{\text{H}} n_{\text{H}} \frac{\Lambda_{tot}}{H_{tot}}, \quad (4)$$

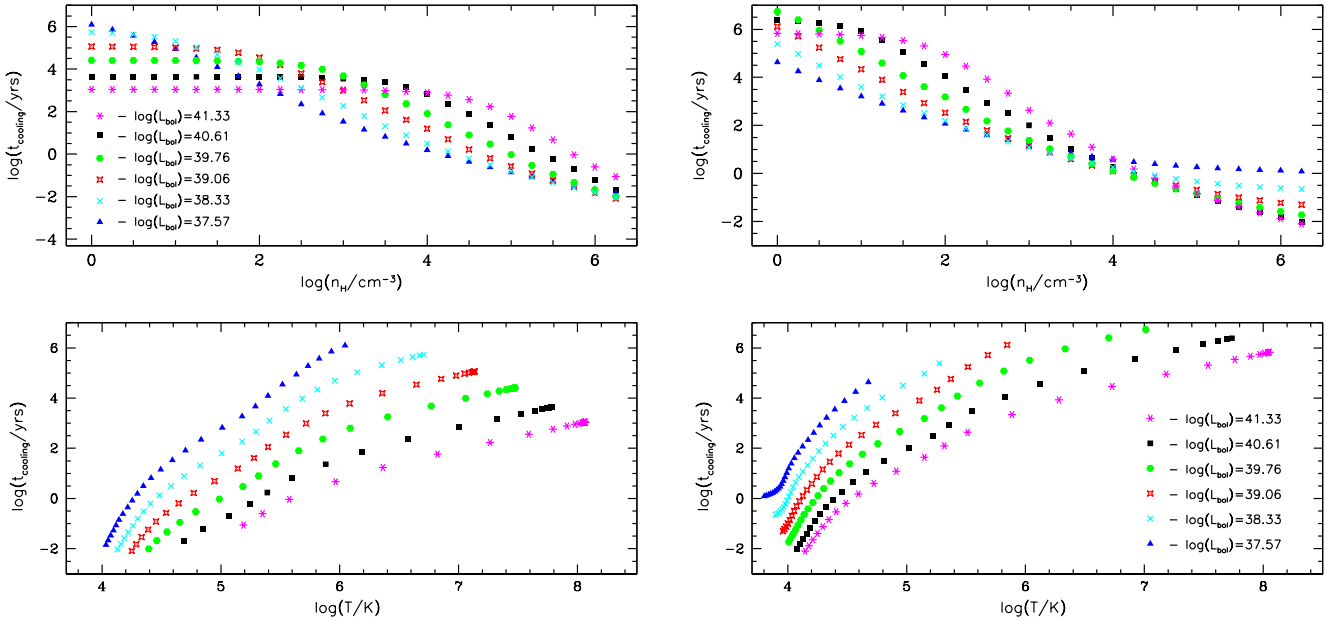


Figure 3. The comparison of cooling time of clouds at two different distances from the GC. Left panels show clouds located at $R_{in} = 0.008$, while the right panels clouds located at $R_{in} = 0.2$ as in Fig. reffig:xi. The cooling time versus temperature for different luminosities is presented in the lower panels, while the cooling time versus cloud number density is presented in the upper panels.

where m_H is the mass of hydrogen atom, and V is the physical volume of the cloud in cm^3 .

4 THERMAL INSTABILITIES FOR DIFFERENT STATES OF LUMINOSITY

As a result of Cloudy computations we present the stability curve, for different luminosity states discussed above. In Fig. 1, lower panels, we present the comparison of stability curves for clouds located at two different distances, 0.008 and 0.2 pc from Sgr A*. At the closer distance, the instability is not present if the luminosity of the central source is too low, $\log(L_{bol}) < 39.06$. However, it operates for four examples of high luminosities considered in our calculations. Further away from the GC, the instability is present only for the two highest luminosities, Fig. 1 (lower right panel).

From the upper panels of Fig. 1, where we present the dependence of cloud temperature versus their number density, we see that unstable clouds are denser when they are located closer to the Sgr A*.

The comparison of total cooling rate of clouds at two different distances from the GC is shown in Fig. 2. The total cooling rate of each cloud is higher for higher cloud number density (upper panels) and for lower cloud temperature (lower panels). Additionally, the total cooling rate is much higher for clouds located farther away from GC (upper right panel of Fig. 2). The dependence of total cooling rate on number density exhibits the pivoting point, which occurs at different number density, depending on the cloud location. However, it does not seem to have any special physical consequence that could be checked observationally. We address this issue for further theoretical consideration in the future.

Finally, we show in Fig. 3, how total cooling time computed from Eq 2, depends on density and temperature. Typically, clouds

located at 0.008 pc from Sgr A*, and with $n_e < 3 \times 10^4 \text{ cm}^{-3}$ can survive more than 100 years (upper left panel of Fig. 3). The cooling time is longer for higher luminosity state, but for high temperature clouds it saturates at the lower value. For the $\log(L_{bol}) = 37.57$, the coolest cloud has the highest possible lifetime $t_{cooling} = 10^6$ yrs. For more distant clouds, their lifetime is shorter, for the lower luminosity states, but longer for the higher luminosity states (right panels of Fig. 3). Still clumps at $n_e < 10^3 \text{ cm}^{-3}$ can survive more than 100 years.

Comparing this approximate cloud cooling time to the timescale of free fall of the cloud onto the supermassive black hole in the GC, we can determine the inner distance R_{min} from the Sgr A*, at which $t_{ff} = t_{cooling}$.

$$R_{min} = \left(\frac{2}{\pi} * t_{cooling} * [2G(M_{BH} + M_{cl})]^{1/2} \right)^{2/3} \quad (5)$$

where G is a gravitational constant, and mass of the cloud, M_{cl} , is negligible in comparison with M_{BH} . If we are interested in clouds living minimum 100 years, they should be visible at distances equal or higher than $R_{min} = 0.054$ pc. It is in good agreement with observations of mini-spiral which is visible down to $\sim 0.1 - 0.2$ pc towards the central black hole. Clouds located closer to the black hole than the calculated value of R_{min} , fall onto black hole before the end of their cooling time.

The extent of the instability depends on the extension of two-phase medium visible on the stability curve. As seen in Fig. 1, lower left panel, for the highest four luminosity states the instability range equals: 0.77, 0.46, 0.26 and 0.07 in terms of $\log(\Xi)$.

At the intermediate distance, 0.08 pc, the stability curves for the same luminosity states are showing that in case of three highest luminosities two-phase medium can arise (Fig. 5, upper panel). Following stability curves, computed for all three distances, it is clear

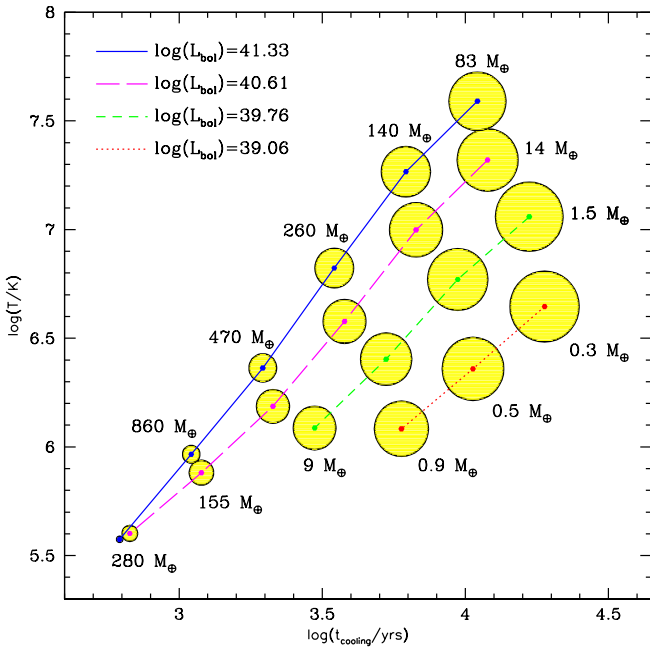


Figure 4. The size of clouds along the instability branch positioned in the log-log plot of cooling time t_{cooling} vs. temperature T . Four different curves are plotted for different values of bolometric luminosity, i.e., the four lines connect clouds that are produced by the same radiation field, as specified in the top-left corner of the plot. Along each curve, the radius of yellow circles represents the Field length according to Eq. 3. Masses of clouds determined by Eq. 4 are given in the units of Earth mass.

that for the same gas physical parameters, the strongest instability occurs closest to the radiation source.

Interestingly, the size of the instability, i.e. the range of ionisation parameter where thermal instability operates, is the same at all three distances if we compare the same luminosity states, even if densities are different. Therefore, we conclude that particular thermal instability can operate far away from GC, and create two-phase medium, if the number density of matter allows it. We check this prediction in Sec. 5.

4.1 The size of clouds

In Fig. 4 we present the overview of clouds being on unstable branch for those luminosity states where instability occurs. Depending on luminosity, clouds have different sizes and masses. We connected by lines those clumps which are produced by the radiation field of the same intensity.

The size of the clouds is given by the Field length of each cloud (Eq. 3), and since there is a difference by many orders of magnitude we presented it in logarithmic scale. The largest clouds have a radius of the order of 10^{17} cm, and they appear either for low luminosity states or for high temperature i.e. low density clouds. Those clouds have the smallest mass reaching even $0.3M_{\oplus}$. The heaviest compact clouds are created for low temperatures and high densities of the order of 10^5 cm^{-3} . They have radii approximately 10^{12} cm, and can accumulate huge mass of the order of few hundred Earth masses.

Unstable clouds with mass of about $10 M_{\oplus}$ can exist even more than ten thousand years. Those are very good candidates for a G2-type cloud in agreement with the recent mass estimation of 4 – 10 M_{\oplus} given by Shcherbakov (2014).

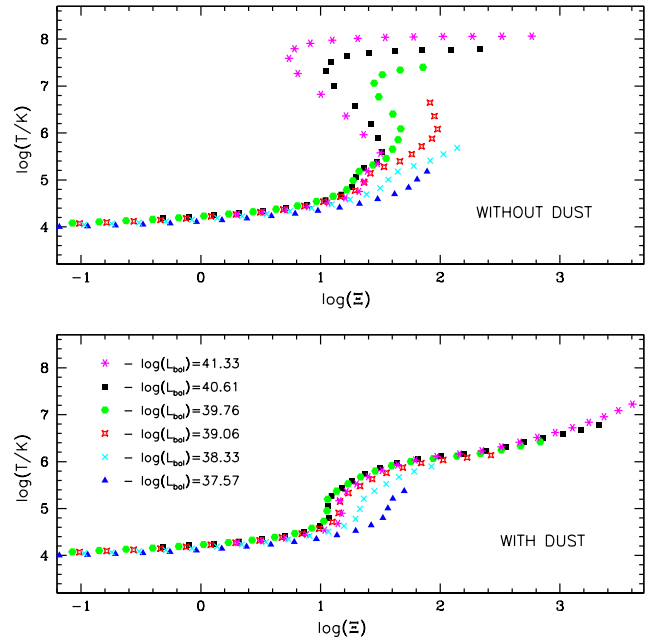


Figure 5. The comparison of stability curves computed without dust and with dust for clouds of the same physical parameters and for the same luminosity states as in previous figures. All clouds presented at upper and lower panels are located at moderate distance 0.08 pc from GC.

4.2 The effect of the dust

Strong extinction towards Sgr A* has been interpreted as a result of the line-of-sight absorption by the intervening material with a significant contribution from interstellar dust grains (Krishna Swamy 2005). Dust in the GC can be formed mainly in atmospheres of cool stars through the process of mass loss and via supernovae explosions that have occurred in the region and helped to disperse the grains into the ISM. Alternatively, the dust can also originate at larger distances from the centre, where the conditions for nucleation are favourable and the material can be transported towards the centre in filaments and clouds. However, these must interact with the wind from hot He stars and the likely wind from Sgr A*. Therefore, the role of dust should be explored in the context of the proposed thermal instability and the structure formation near the supermassive black hole.

Order-of-magnitude estimates indicate the typical interstellar dust-to-gas ratio about $\sim 1\%$ is maintained. Complexities of the thermal structure and stratification in the GC region have been revealed by infrared absorption features (e.g. Gibb et al. 2004; Moultaqa et al. 2009, based on ISO satellite observations, and based on ESO’s VLT M -band spectra, respectively). These have been identified as shocks and filaments that develop in the region. Bow shocks presumably originate from the interaction of stars embedded in the ISM of the GC (Clénet et al. 2004; Mužić et al. 2010), which points to the importance of stars as an additional source of energy. Therefore, conditions for dust formation are particularly varied through the central region.

The thermal instability is not the only mechanism that can enhance mixing and, consequently, drive accretion in the complex environment. Moreover, the abundance of heavy elements generally increases towards the GC, so a higher dust-to-gas ratio can be expected. This raises a question whether the presence of dust could suppress the instability close to the black hole by acting as an ef-

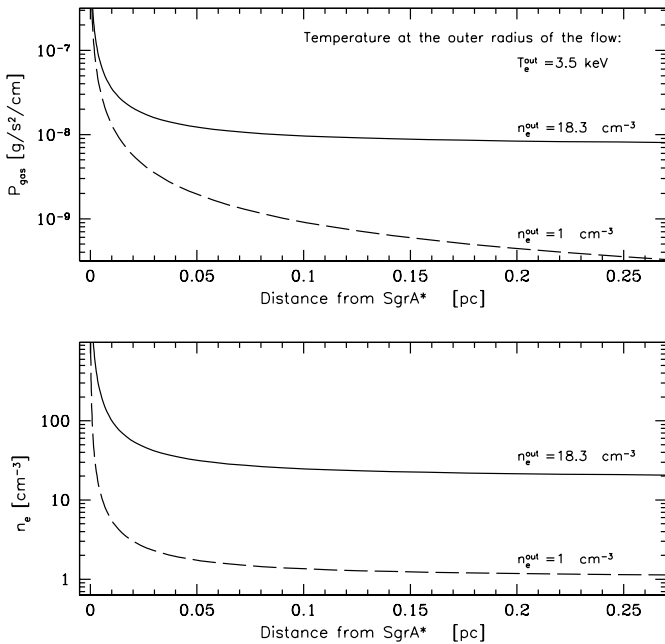


Figure 6. The gas pressure profile (upper panel), and density profile (lower panel) for hot phase, in case of Bondi accretion flow with $T_e^{\text{out}} = 3.5$ keV as it was found in X-ray data. Two values of outer number density are considered. From the best fitting model $n_e^{\text{out}} = 18.3$ cm^{-3} – solid line, and for the large extent of instability $n_e^{\text{out}} = 1$ cm^{-3} – dashed line.

efficient heat sink. On the other hand, dusty plasma is known to become unstable by a variety of instability modes that are driven under external action, depending on the actual chemical composition and size of dust grains (see Mendis & Rosenberg 1994; Cox 2005; Vladimirov & Ostrikov 2005; Zajaček et al. 2014, and further references cited therein). In addition, irradiated by UV/X-ray photons and embedded in the plasma dust grains must acquire a significant electric charge (Ishihara 2007). The presence of charged dust in the plasma modifies the usual instabilities and the electrostatic repulsion can even contribute to erosion and rapid destruction of dust.

In our computations discussed in the previous section we neglected the existence of dust. Observations show clearly that, at present, the mini-spiral also contains dust (Mužić et al. 2007). Therefore, we performed the computations of the thermal instability $\log(\Xi) - \log(T)$ curve with the dust grain option included in Cloudy, assuming the standard dust composition characteristic for the interstellar medium. The effect is illustrated in Fig. 5, where we compare the stability curves for the same physical parameters with dust (lower panel), and without dust (upper panel) at a moderate distance of 0.08 pc, i.e. $2''$ or $\log(R) = 17.39$ cm, from GC.

The low temperature branch, with the temperatures well below $T \sim 10^5$ K is unaffected by the presence of the dust. High temperature part of the diagram is strongly modified: the gas temperature is much lower since the dust intercepts significant fraction of the incident radiation. The dust temperature, even for the very high luminosity, is still moderate, $T_{\text{dust}} \sim 300$ K so the high level of Sgr A* activity does not destroy the dust radiatively. However, it is well known that hot surrounding plasma easily destroys the dust particles collisionally (e.g. Draine & Salpeter 1979). In particular, recent computations of the dust particle erosion in a hot gas by Bocchio et al. (2012, 2013) indicate the destruction timescale of 10 years for a hot plasma number density of 10 cm^{-3} . This means, that the dust survives only within the warm medium clouds, where

it does not affect the temperature much, and vanishes immediately from the hot phase. Thus, the stability curve for the dustless plasma applies for timescales larger than a year. On the other hand, on shorter timescales the effect of dust is visible (Krabbe et al. 1995) especially if its efficient formation in stellar winds replenishes the dust content at a sufficiently fast rate to ensure the steady state.

5 TWO-PHASE MEDIUM IN BONDI FLOW AROUND SGR A*

From the fitting of X-ray data surface brightness profile, it was found that Bondi accretion operates up to 0.12 pc from Sgr A* (Różańska et al. 2014, in preparation). Further away hot plasma is interacting with stars and the more advanced dynamical model, where Bondi flow is mixed with stars, fits better as shown by Shcherbakov & Baganoff (2010), where fit to *Chandra* data was done up to 0.2 pc.

For this paper, we adopt that the hot plasma in the mini-spiral region is well represented by Bondi accretion flow. We assumed here, that the inner hot accretion flow, for which luminosity states were computed (Sec. 3.1) changes to the Bondi flow for larger distances with zero angular momentum. This is in agreement with the work done by Cuadra et al. (2008), where the circularized radius was estimated on $R_{\text{circ}} \sim 0.002$ pc. For the Bondi accretion flow starting roughly at the capture radius, we were able to compute density and gas pressure profile around Sgr A*, with initial parameters $T_e^{\text{out}} = 3.5$ keV, and $n_e^{\text{out}} = 18.3$ cm^{-3} , defined on the outer radius of the flow (far above 2 pc) taken from observations (Różańska et al. 2014, in preparation).

In Fig. 6, we present the gas pressure and the number density profiles versus distance from the black hole for the Bondi accretion. We consider one outer temperature and two outer number densities: $n_e^{\text{out}} = 18.3$ cm^{-3} , and $n_e^{\text{out}} = 1$ cm^{-3} .

Finally, Fig. 7 represents instability strips computed for both models respectively. For each luminosity state at each distance we calculated the value of Ξ parameter taking into account gas pressure and density number profiles for both cases of Bondi flows. The instability strips are marked as magenta colour for each luminosity state.

The occurrence of instability during the high-luminosity history of Sgr A*, and its disappearance at the present low-luminosity stage, represent the main argument of this paper. For all gas above the red contour, only hot phase can exist at a given luminosity. For the matter below the blue contour, only cold clouds can exist. There are several distance ranges where two-phase medium can co-exist. Nevertheless, for Bondi flow with $n_e^{\text{out}} = 18.3$ cm^{-3} (left panel of Fig. 7) it appears only for two highest luminosities and quite close to the Sgr A* within 0.4 pc. In case of Bondi flow with $n_e^{\text{out}} = 1$ cm^{-3} (right panel of Fig. 7) two-phase medium can be sustained up to 1.4 pc.

6 DISCUSSION

Our estimates presented in this paper are clearly oversimplified, since we did not include the additional heating of the medium by stars, which explains observed X-ray brightness profile above 0.12 pc (Shcherbakov & Baganoff 2010). Such an additional heating may slightly shift the instability region but in general it enhances the instability.

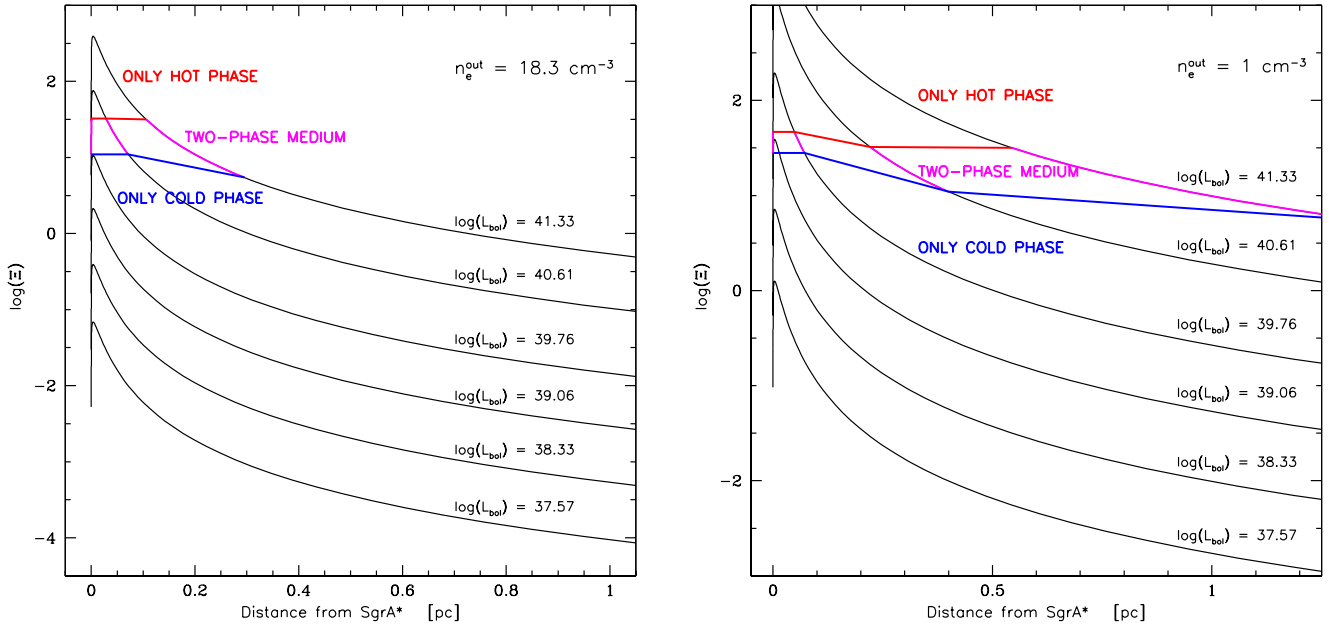


Figure 7. Instability strips for the different luminosity states in case of Bondi accretion flow onto Sgr A* for outer temperature $T_e^{\text{out}} = 3.5$ keV. Left panel shows cases for outer number density $n_e^{\text{out}} = 18.3 \text{ cm}^{-3}$ and right panel for $n_e^{\text{out}} = 1 \text{ cm}^{-3}$. The region in between colour contours is the two phase-medium, and its extent is shown by magenta lines for each luminosity state. The thermal instability can operate in range of high luminosity for Sgr A*, which occurred in its past history.

The multi-phase character of the medium affects to some extent the accretion pattern, as showed by Barai et al. (2011, 2012), and Mościbrodzka & Proga (2013). The main effect can be easily seen from consideration of the simplest spherically symmetric Bondi accretion flow. The Bondi radius for the hot plasma is of order of

$$R_{\text{Bondi}}^{\text{hot}} = 0.074 q_s \frac{M_{\text{BH}}}{4.5 \times 10^6 M_{\odot}} [\text{pc}], \quad (6)$$

where the sound speed for the hot material has been set to 500 km s^{-1} and q_s coefficient depends on the adopted polytropic index γ . If $q_s = 1$, the inner edge of the mini-spiral is close to that radius. However, for $\gamma = 1.6$, $q_s = 0.05$ and the hot material at the inner radius of the mini-spiral is not yet flowing in.

For the cold material, the square of the sound speed is by a factor of 10^3 lower so the infall is possible even from larger distances than the inner edge of the mini-spiral, as the formal Bondi radius for would be three orders of magnitude larger

$$R_{\text{Bondi}}^{\text{hot}} = 3.7 \frac{M_{\text{BH}}}{4.5 \times 10^6 M_{\odot}} [\text{pc}]. \quad (7)$$

Here we adopted $\gamma = 1.6$. Therefore, the cold material falls immediately into the black hole as soon as it loses its angular momentum. This is exactly the pattern seen in the numerical computations: cold clumps may accrete when the hot medium which surrounds them, is outflowing due to the strong heating.

The dynamics of the mini-spiral is even more complicated since its material possesses a significant amount of angular momentum (Zhao et al. 2009). However, clouds can lose angular momentum in the collisions. The mutual collisions lead to the gradual dissipation of angular momentum, so that the individual clouds are expected to fall more rapidly to the center. Also the radiation drag by the central source and the luminous inner accretion disc act on

the cloud to change the ratio of azimuthal versus radial velocity components. For clouds of sufficiently large optical thickness, the shape and stability of their orbits is strongly affected by the radiation pressure especially during the luminous phase of the centre (e.g. Fukue & Hachiya 1999; Ghisellini et al. 2004). The radial component of the motion then starts to grow relative to purely angular component, as was studied, including the relativistic effects acting on the motion (Abramowicz et al. 1990; Vokrouhlicky & Karas 1991). The properties of particle motion can be employed to effectively represent the cloud mean motion, however, different aspects (such as the role of the cloud internal temperature) have been also discussed (Keane et al. 2001; Horák & Karas 2006). It has been shown that in case of more general (non-radial) orbits, although the shape of bound trajectories deviates from ellipses, the motion remain closed (Plewa et al. 2013). Therefore, we assume that non-gravitational effects contribute to higher-order corrections and remain beyond the scope of the present paper. Furthermore, Cuadra et al. (2005) have studied the expected properties of the process accretion of cool stellar winds on to Sgr A* supermassive black hole. These authors notice that cool streams of gas frequently enter this region on low angular momentum orbits. Then the streams are disrupted and heated up to the ambient hot gas temperature.

Cloudy photoionisation computations allow to search for the influence of dust and cosmic rays on the thermal instability. The dust was extensively discussed in the previous section. We have made test on how typical cosmic ray background can change the shape of stability curve, and we did not observe even small effect.

It was shown in the original paper (Field 1965) that the presence of the magnetic field penetrating the electrically conducting gaseous medium leads to several different effects that can modify the conditions for the thermal (non-gravitational) instability.

Firstly, the internal pressure gets increased by the additional magnetic influence, so the pressure term must be replaced by the sum of gas plus magnetic terms (Langer 1978). Next, the presence of the magnetic field leads to an anisotropic heat flow since the motion of electrons is greatly reduced in the direction across the field lines. However, in the plane-parallel approximation the growth timescale of the condensation instability is not diminished strongly, unless the magnetic field is strictly perpendicular to the temperature gradient (Field 1965; van Hoven & Mok 1984). This may not be true in a complete (three-dimensional) picture since the magnetisation will likely lead to the creation of complex filamentary structures. Hence, advanced numerical simulations must include this anisotropic term (Sharma & Hammett 2007; Parrish et al. 2009). Furthermore, suppression of thermal conductivity in the direction normal to field lines depends on the state of the medium, i.e., the case of fully vs. partially ionized gas. Furthermore, Burkert & Lin (2000) found that tangled magnetic fields can reduce the conductive heat flux enough for low-amplitude fluctuations to grow and become non-linear if their length scales are of order ~ 0.01 pc. These authors argue that if the amplitude of the initial perturbations is a decreasing function of the wavelength, the size of the emerging clumps will also decrease with increasing strength of the magnetic field.

Therefore, the clumpiness of the mini-spiral medium caused by the thermal instability creates a possibility of episodes with enhanced accretion of cold clumps towards Sgr A* and may well explain its enhanced activity in the past.

7 CONCLUSIONS

The central region of the Milky Way consists of the supermassive black hole, a hot X-ray emitting plasma filling roughly uniformly the space, and the filaments of the colder gas and dust. Some of these filaments, in the form of the mini-spiral, extend down to $\sim 0.1 - 0.2$ pc towards the central black hole. Here we analyzed a possibility that the two-phase medium in the mini-spiral region close to Sgr A* might have formed due to the thermal instability which can develop in the irradiated medium.

We showed that the current level of the X-ray emission from the vicinity of Sgr A* is not high enough to drive the thermal instability. However, there are strong arguments that Sgr A* was orders of magnitude brighter in the past, about a hundred years ago. In that case, for central luminosities higher than $\sim 10^{39}$ erg s^{-1} , in the medium at distances 0.008 - 0.2 pc, the instability operates and the heated medium spontaneously forms colder clumps embedded in the hot low density plasma. Such two-phase medium exists for hundreds of years after the turnoff of the nuclear emission since the cooling timescale of the hot gas is very long. We have shown that clouds located at distance higher than 0.054 pc from Sgr A*, can survive hundreds years, since this cooling/evaporation time is shorter than free fall time at this distance. Clouds located closer toward the GC will first fall onto black hole rather than evaporate.

Thermal instability mechanism explains in the natural way the gas pressure equilibrium between the hot and the cold plasma. It also allows to estimate the typical size of the cold clump to be of the order of 10^{14-15} cm, and the total mass of about 10 Earth masses. It will change with the shape and strength of radiation field. But it agrees with recent results by Shcherbakov (2014), who suggested mass for G2 cloud from 4 to 20 M_{\oplus} .

We computed most of the results not taking dust into consideration but we showed that the presence of the dust does not change our main conclusions. The temperature of the cold clumps is not

affected by dust, since the atomic cooling is also very efficient at temperatures $\sim 10^4$ K. The presence of the dust is extremely important for the hot material, but the dust embedded in a hot plasma is collisionally destroyed in a timescale of a year and after that we only expect the coexistence of the cold dusty phase and a hot dustless plasma.

ACKNOWLEDGMENTS

This research was supported by Polish National Science Centre grants No. 2011/03/B/ST9/03281, 2013/10/M/ST9/00729, and by Ministry of Science and Higher Education grant W30/7.PR/2013. It received funding from the European Union Seventh Framework Program (FP7/2007-2013) under grant agreement No.312789. D.K. and V.K. acknowledge support from the collaboration project between the Czech Science Foundation and Deutsche Forschungsgemeinschaft (GACR-DFG 13-00070J).

REFERENCES

- Abramowicz M. A., Ellis G. F. R., Lanza A., 1990, *ApJ*, 361, 470
 Alig C., Schartmann M., Burkert A., Dolag K., 2013, *ApJ*, 771, 119
 Baganoff F. K., et al., 2003, *ApJ*, 591, 891
 Barai P., Proga D., Nagamine K., 2011, *MNRAS*, 418, 591
 Barai P., Proga D., Nagamine K., 2012, *MNRAS*, 424, 728
 Begelman M. C., McKee C. F., 1990, *ApJ*, 358, 375
 Begelman M. C., McKee C. F., Shields G. A., 1983, *ApJ*, 271, 70
 Bocchio M., Micelotta E. R., Gautier A.-L., Jones A. P., 2012, *A&A*, 545, A124
 Bocchio M., Jones A. P., Verstraete L., Xilouris E. M., Micelotta E. R., Bianchi S., 2013, *A&A*, 556, A6
 Burkert A., Lin D. N. C., 2000, *ApJ*, 537, 270
 Capelli R., Warwick R. S., Porquet D., Gillissen S., Predehl P., 2012, *A&A*, 545, A35
 Christopher M. H., Scoville N. Z., Stolovy S. R., Yun M. S., 2005, *ApJ*, 622, 346
 Clénet Y., et al., 2004, *A&A*, 417, L15
 Cotera A., Morris M., Ghez A. M., Becklin E. E., Tanner A. M., Werner M. W., Stolovy S. R., 1999, in Falcke H., Cotera A., Duschl W. J., Melia F., Rieke M. J., eds, *Astronomical Society of the Pacific Conference Series Vol. 186, The Central Parsecs of the Galaxy*. p. 240
 Cowie L. L., McKee C. F., 1977, *ApJ*, 211, 135
 Cox D. P., 2005, *ARA&A*, 43, 337
 Cuadra J., Nayakshin S., Springel V., Di Matteo T., 2005, *MNRAS*, 360, L55
 Cuadra J., Nayakshin S., Martins F., 2008, *MNRAS*, 383, 458
 Czerny B., Karas V., Kunneriath D., Das T. K., 2013a, in Zhang C. M., Belloni T., Méndez M., Zhang S. N., eds, *IAU Symposium Vol. 290, IAU Symposium*. pp 199–200
 Czerny B., Kunneriath D., Karas V., Das T. K., 2013b, *A&A*, 555, A97
 Draine B. T., Giuliani Jr. J. L., 1984, *ApJ*, 281, 690
 Draine B. T., Salpeter E. E., 1979, *ApJ*, 231, 77
 Ferland G. J., et al., 2013, *Rev. Mexicana Astron. Astrofis.*, 49, 137
 Field G. B., 1965, *ApJ*, 142, 531
 Fukue J., Hachiya M., 1999, *PASJ*, 51, 185

- Gezari D. Y., Shu P., Lamb G., Tresch-Fienberg R., Fazio G. G., Hoffmann W. F., Gatley I., McCreight C., 1985, *ApJ*, 299, 1007
- Ghez A. M., et al., 2008, *ApJ*, 689, 1044
- Ghisellini G., Haardt F., Matt G., 2004, *A&A*, 413, 535
- Gibb E. L., Whittet D. C. B., Boogert A. C. A., Tielens A. G. G. M., 2004, *ApJS*, 151, 35
- Gillessen S., Eisenhauer F., Trippe S., Alexander T., Genzel R., Martins F., Ott T., 2009, *ApJ*, 692, 1075
- Hess C. J., Kahn S. M., Paerels F. B. S., 1997, *ApJ*, 478, 94
- Horák J., Karas V., 2006, *MNRAS*, 365, 813
- Ishihara O., 2007, *Journal of Physics D Applied Physics*, 40, 121
- Keane A. J., Barrett R. K., Simmons J. F. L., 2001, *MNRAS*, 321, 661
- Koyama K., Maeda Y., Sonobe T., Takeshima T., Tanaka Y., Yamauchi S., 1996, *PASJ*, 48, 249
- Krabbe A., et al., 1995, *ApJ*, 447, L95
- Krishna Swamy K. S., 2005, *Dust in the universe : similarities and differences*
- Krolik J. H., McKee C. F., Tarter C. B., 1981, *ApJ*, 249, 422
- Langer W. D., 1978, *ApJ*, 225, 95
- Liszt H. S., 2003, *A&A*, 408, 1009
- McKee C. F., Cowie L. L., 1977, *ApJ*, 215, 213
- Mendis D. A., Rosenberg M., 1994, *ARA&A*, 32, 419
- Mościbrodzka M., Proga D., 2013, *ApJ*, 767, 156
- Mościbrodzka M., Shiokawa H., Gammie C. F., Dolence J. C., 2012, *ApJ*, 752, L1
- Moultaka J., Eckart A., Schödel R., 2009, *ApJ*, 703, 1635
- Mužić K., Eckart A., Schödel R., Meyer L., Zensus A., 2007, *A&A*, 469, 993
- Mužić K., Eckart A., Schödel R., Buchholz R., Zamaninasab M., Witzel G., 2010, *A&A*, 521, A13
- Parrish I. J., Quataert E., Sharma P., 2009, *ApJ*, 703, 96
- Plewa P. M., Schartmann M., Burkert A., 2013, *MNRAS*, 431, L127
- Ponti G., Terrier R., Goldwurm A., Belanger G., Trap G., 2010, *ApJ*, 714, 732
- Różańska A., 1999, *MNRAS*, 308, 751
- Różańska A., Czerny B., 1996, *Acta Astron.*, 46, 233
- Różańska A., Mróz P., Mościbrodzka M., Sobolewska M., Adhikari T. P., 2014, in preparation
- Sharma P., Hammett G. W., 2007, *Journal of Computational Physics*, 227, 123
- Shcherbakov R. V., 2014, *ApJ*, 783, 31
- Shcherbakov R. V., Baganoff F. K., 2010, *ApJ*, 716, 504
- Sunyaev R. A., Markevitch M., Pavlinsky M., 1993, *ApJ*, 407, 606
- Vladimirov S. V., Ostrikov K., 2005, in Boufendi L., Mikikian M., Shukla P. K., eds, *American Institute of Physics Conference Series Vol. 799, New Vistas in Dusty Plasmas*. pp 446–449
- Vokrouhlicky D., Karas V., 1991, *A&A*, 252, 835
- Vollmer B., Duschl W. J., 2002, *A&A*, 388, 128
- Zajaček M., Karas V., Eckart A., 2014, *A&A*, 565, A17
- Zhao J.-H., Morris M. R., Goss W. M., An T., 2009, *ApJ*, 699, 186
- Zhao J.-H., Blundell R., Moran J. M., Downes D., Schuster K. F., Marrone D. P., 2010, *ApJ*, 723, 1097
- van Hoven G., Mok Y., 1984, *ApJ*, 282, 267